Design and Analysis of Two Ultra-Fast All-Optical Plasmonic Dual- Band OFF-ON and Bi-Directional Switches Based on Nonlinear Kerr Materials

MOHAMMADREZA PAV
K.N. Toosi University of Technology
siavash pooretemad
K.N. Toosi University of Technology
NOSRAT GRANPAYEH (granpayeh@kntu.ac.ir)
K.N. Toosi University of Technology

Research Article

Keywords: Nonlinear OFF-ON plasmonic switches; bi-directional plasmonic switches, nonlinear Kerr materials, bistability effect, self-phase modulation (SPM)

Posted Date: June 27th, 2023

DOI: https://doi.org/10.21203/rs.3.rs-3078981/v1

Additional Declarations: No competing interests reported.

Design and Analysis of Two Ultra-Fast All-Optical Plasmonic Dual-Band OFF-ON and Bi-Directional Switches Based on Nonlinear Kerr Materials

MOHAMMADREZA PAV, SIAVASH POORETEMAD, AND NOSRAT GRANPAYEH*

Center of Excellence in Electromagnetics, Optical Communication Laboratory, Faculty of Electrical Engineering, K.N. Toosi University of Technology, Tehran, Iran
**granpayeh@kntu.ac.ir*

Abstract: In this study, two ultra-fast all-optical plasmonic switches based on metal–insulator–metal (MIM) plasmonic waveguides side-coupled to cavity by stubs are proposed. The cavities are filled with a nonlinear Kerr material and the switching occurs due to the self-phase-modulation (SPM) effect. In the first structure, an OFF-ON switching functionality is achieved either by varying the incident light intensity or using the optical bistability effect at the two telecommunication windows of 1550 nm and 850 nm. In the second structure, by adding another nonlinear cavity a bi-directional switch is designed. The finite-deference time-domain (FDTD) method is used to obtain the simulation results. The proposed ultra-fast switches have significant switching mechanisms and picosecond response time (0.25ps for the Off-ON switch and 1.5ps for the bi-directional switch). The proposed all-optical switches have potential of significant applications in photonic integrated circuits (PICs).

Keywords: Nonlinear OFF-ON plasmonic switches; bi-directional plasmonic switches, nonlinear Kerr materials, bistability effect, self-phase modulation (SPM).

1 Introduction

A major challenge in miniaturization of high-density photonic integrated circuits is caused by the well-known diffraction limit [1]. Surface plasmon polaritons (SPPs) are a type of transverse electromagnetic waves which are tightly confined at a metal-dielectric interface and can guide light and overcome the diffraction limit [2]. Metal-insulator-metal (MIM) and insulator-metal-insulator (IMI) waveguides are two types of plasmonic subwavelength structures which are commonly used for guiding the SPPs [3]. The MIM waveguides have more confined electromagnetic fields, but higher loss compared to the IMI waveguides [3].

To construct the MIM structures the standard silicon-on-insulator (SOI) wafers are usually used. Moreover, the electron-beam lithography (EBL), metal deposition and liftoff are utilized to fabricate these plasmonic structures [4-5]. In MIM structures, their different parts such as input and output waveguides, apertures, and cavities, have different widths usually ranging from wide (200nm or more) to small (around 25nm) [5-7]. Since the dimensions of these structures are far from the sub-nanometer scales, from which quantum phenomena occur, quantum theory is not necessary for the analysis of them. This was also proven by Campos [8] and Ciraci [9] that only for structures with dimensions smaller than 10nm, the optical response is affected by the quantum phenomena.

Two different practical methods for coupling electromagnetic waves into MIM structures have been explained in [4, 5]. It was demonstrated that plasmonic structures with MIM waveguides, can split input power almost perfectly without introducing additional reflection and radiation loss beyond the inherent Ohmic loss of the straight waveguide. The reflection can even be reduced by rounding the sharp corners and hence increasing slightly the bending radius of the curvature. Therefore, basic waveguide components such as sharp 90° bends and T-splitters can be constructed in plasmonic waveguides as a simple and compact structure [10]. Due to several advantages such as simple fabrication, easy integration, and subwavelength mode confinement, plasmonic structures with MIM configuration have been investigated for a wide range of applications such as filters and switches [11-15], multiplexers-demultiplexers [16-17], power

dividers [18-19], sensors [20-24], etc. Due to more field confinement and consequently higher electrical field intensities in plasmonic structures compared to their counterparts in conventional optics, nonlinear optical phenomena in plasmonic devices can be achieved at lower threshold intensities [25]. A Kerr material is a third order nonlinear material which its refractive index can be altered due to the self-phase-modulation (SPM) effect which is caused by a high intensity incident wave [26]. During past decade, numerous all-optical switches have been designed operating based on the SPM effect [27-30]. Another nonlinear phenomenon investigated for design of all-optical switches is the optical bistability effect [31-34]. In this phenomenon, the system has two stable states.

In this study, a structure with MIM plasmonic waveguides side-coupled to a rectangular cavity by a stub has been designed. The cavity is filled with a nonlinear Kerr material. Using the electromagnetic field equations inside the cavity and the relation between the resonance wavelengths and the geometrical parameters of the cavity, a band-pass filter can be achieved at two wavelengths slightly lower than the two telecommunication windows of 1550 nm and 850 nm, so that the transmission at these two windows is near zero (OFF-state). By increasing the incident wave intensity, the refractive index of the nonlinear material inside the cavity increases due to the Kerr effect. Consequently, the transmission spectrum shifts towards longer wavelengths (a red shift) so that the amplitudes at the two telecommunication windows of 1550 nm and 850 nm increase from near zero to higher values (ON-state). Therefore, a dual-wavelength all-optical OFF-ON plasmonic switch operating based on varying the intensity of the incident light has been designed. Moreover, the bistability effect for the proposed switch has been investigated. The simulation results show that the structure has a wide bistability loop; therefore, the switching operation is possible in a wider range of input intensities and consequently tuning the applied intensity for optimized performance is practical. Therefore, the switching operation can also be realized by the optical bistability phenomenon. In addition, an all-optical bi-directional switch by adding another nonlinear cavity to the previous structure has been designed. The proposed switch operates based on increasing the incident wave intensity which causes the input power to switch between the two output ports. The proposed structures are ultra-compact and have significant ultra-fast switching performance of picosecond response times of 0.25ps for the OFF-ON switch and 1.5ps for the bi-directional one. Our proposed switching structures are more compact than other types and require less input power intensity for switching operation. In addition, our proposed structures have several advantages such as simple fabrication, easy integration, and subwavelength mode confinement. Therefore, the proposed all-optical switches have potential of significant applications in photonic integrated circuits. For the numerical simulation results, the two-dimensional (2D) finite-deference time-domain (FDTD) method has been used.

The remaining of the paper is organized as follows. The structure design and the analysis methods are described in Section 2. In Section 3, an ultra-fast all-optical plasmonic dual-band OFF-ON switch based on varying the intensity is proposed and the results are discussed. In Section 4, an investigation on the bistability effect of the proposed ultra-fast all-optical plasmonic OFF-ON switch is presented. Moreover, an ultra-fast all-optical plasmonic bi-directional switch is designed and analyzed in Section 5. Finally, the paper is concluded in Section 6.

2 Structure Design and Analysis Methods

The two-dimensional schematic view of our first proposed structure is shown in Fig. 1(a). The white area indicates air and the background area (blue color) is assumed to be silver (Ag). To design our proposed switches, the cavity is filled with a nonlinear Kerr material (orange color). The structure is investigated in wavelength range of 600-1800 nm. The imaginary part of the refractive index of silver, derived from Drude model [35] or experimental data [36], has small differences for photon energies below 1.6eV (wavelengths above 800nm) and large differences

in photon energies above 1.6eV (wavelengths bellow 800nm). Since the Drude model is not accurate for wavelengths lower than 800nm, we have used the experimental refractive indices of silver from [36] in our simulations to achieve much more accurate results.

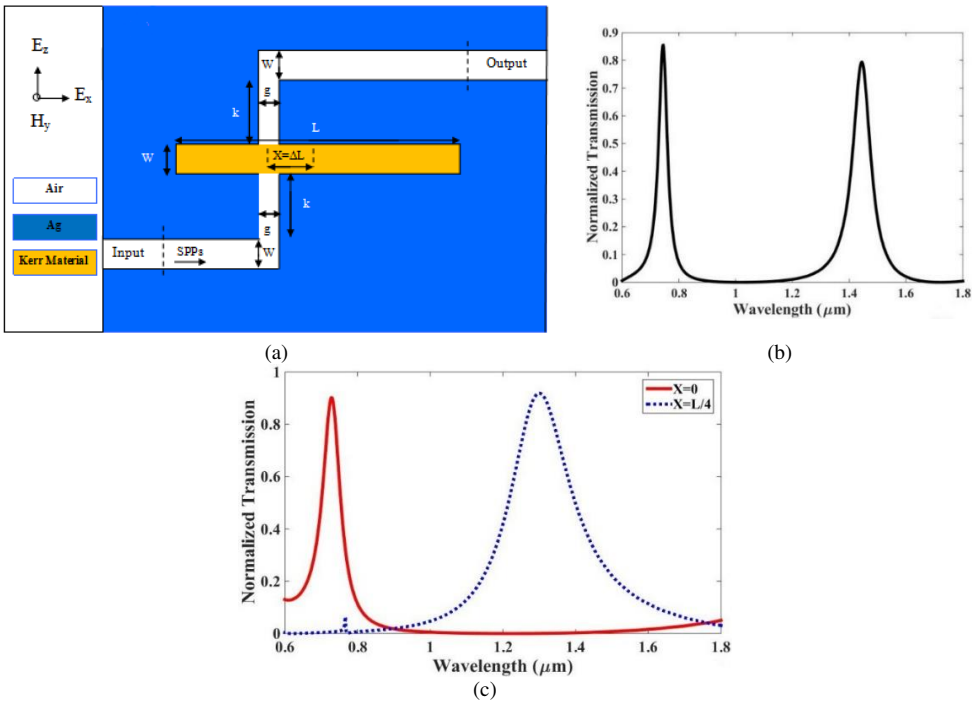

Fig. 1. (a) The two-dimensional building block of the proposed plasmonic OFF-ON switch structure. (b) Normalized transmission of the structure when the position of the stubs is set as $X=\Delta L=L/8$ and the incident wave intensity is low. (c) Comparison of the normalized transmission for two different values of the position of the stubs: $X=\Delta L=0$ (solid red line) and $X=\Delta L=L/4$ (dotted blue line).

The 2D-FDTD method is employed for simulation of our proposed structures, which are assumed to be infinite in one dimension, in order to reduce the simulation time for testing the performance of the devices [37]. However, the thickness of the waveguide must be considered for practical applications, since it has a significant effect on the loss of the device. As discussed in [38], for a specific wavelength range, for the thickness of the MIM waveguide higher than a certain value, the effective refractive index of the structure does not vary and since the loss of the structure is related to the imaginary part of the effective refractive index, the loss of the structure will be constant. Therefore, if the thickness is increased more than the certain value n_{eff} will reach the value used in 2D simulations, which the thickness is assumed to be infinite. Hence, the 2D-FDTD method with convolutional perfectly matched layers (CPMLs) as the boundary condition is used for simulation of our proposed structures. The spatial mesh steps in x and y directions are set as $\Delta x = \Delta y = 4\text{nm}$ and due to the Courant condition, the time step is set as: $\Delta t = \dfrac{0.95}{c\sqrt{(\Delta x)^{(-2)} + (\Delta y)^{(-2)}}}$, where c is the free space speed of light. It is assumed that the fundamental transverse magnetic (TM) mode is excited by the incoming pulse at the left end of the input MIM waveguide. The fast Fourier transforms (FFT) of the input and output

fields measured at the input and output ports power monitors (P_{in} and P_{out}) are used to obtain the power transmission spectra.

As shown in Fig. 1(a), our proposed structure is based on MIM plasmonic waveguides side-coupled to a rectangular cavity by stubs. Center of the cavity has a displacement relative to the center of the input (ΔL) and the output (X) stubs, respectively.

When the cavity resonance condition is satisfied, the stable standing waves are appeared within the cavity [38]: $\Delta\varphi = \beta_m \times 2 \times L + \varphi_r = 2m\pi$, where $\varphi_r = \varphi_1 + \varphi_2$, φ_1 and φ_2 are the phase shifts of the wave reflected at the two ends of the cavity, which are negligible and therefore: $\beta_m \times 2L \approx 2m\pi$. The theoretical relation between the resonance wavelength of the m^{th} order mode, λ_{rm} , and the length of the cavity is described as follows [39].

$$\lambda_{rm} = \frac{2n_{eff}L}{m - \frac{\varphi_r}{2\pi}} \approx \frac{2n_{eff}L}{m} \tag{1}$$

where m is a positive integer, $n_{eff} = \beta_m / k_0$ is the effective refractive index, which β_m is the propagation constant of the guided mode, and k_0 is the free space wave number.

The analytical relation for the magnetic field inside the cavity with an arbitrary input $\left(0 \le \Delta L \le \frac{L}{2}\right)$ and output $\left(0 \le x \le \frac{L}{2}\right)$ stub positions is given as follows [40, 41]:

$$H_m(x,t) = \frac{2H_0}{\alpha}\cos\left[\beta_m\left(x - \frac{L}{2}\right)\right]\left\{\exp\left[-j\beta_m\left(\frac{3}{2}L - \Delta L\right)\right] + \exp\left[-j\beta_m\left(\frac{1}{2}L + \Delta L\right)\right]\right\}\exp(j\omega_m t) + C.C. \tag{2}$$

where ω_m is the angular frequency of the SPPs corresponding to the m^{th} order resonance mode of the cavity and α is the loss coefficient of the cavity. For the first (m=1) and the second (m=2) resonance modes, the propagation constant is: $\beta_{m=1} = 2\pi/2L = \pi/L$ and $\beta_{m=2} = 4\pi/2L = 2\pi/L,$ respectively, and therefore, from Eq. 2, the magnetic field distribution for the first and the second resonance modes are:

$$H_1(x,t) = \frac{-4H_0}{\alpha}\sin\left(\frac{\pi}{L}x\right)\sin\left(\frac{\pi}{L}\Delta L\right)\exp(j\omega_1 t) + C.C. \tag{3}$$

$$H_2(x,t) = \frac{4H_0}{\alpha}\cos\left(\frac{2\pi}{L}x\right)\cos\left(\frac{2\pi}{L}\Delta L\right)\exp(j\omega_2 t) + C.C. \tag{4}$$

From above equations, we can conclude that when the stubs are placed in the center of the horizontal cavity ($X=\Delta L=0$), the first mode will be eliminated, and when they are placed at $X=\Delta L=L/4$, the second mode will be eliminated (Fig. 1(c)). Moreover, to have both resonance modes at the output, the first and second stub positions is set between these two amounts: $X=\Delta L=L/8$ (Fig. 1(b)). The magnetic field distributions of the first and the second resonance

modes in Fig. 1(b) are shown in Fig. 2 (a) and Fig. 2 (b), respectively. As shown in Fig. 2(a) and from Eq. 3, the peaks of magnetic fields at the first resonance mode occur at the edges of the resonator. In addition, as shown in Fig. 2(b) and from Eq. 4, the peaks of magnetic fields at the second resonance mode occur both at the center and at the edges of the resonator. Therefore, when position of the stubs is between $X=\Delta L=0$ and $X=\Delta L=L/4$, when it is shifted towards (backwards) the center of the resonator, the amplitude of the second mode will become higher (lower) but the amplitude of the first mode will become lower (higher). Thus, the stubs are placed at $X=\Delta L=L/8$ to have rather high amplitudes for both resonance modes.

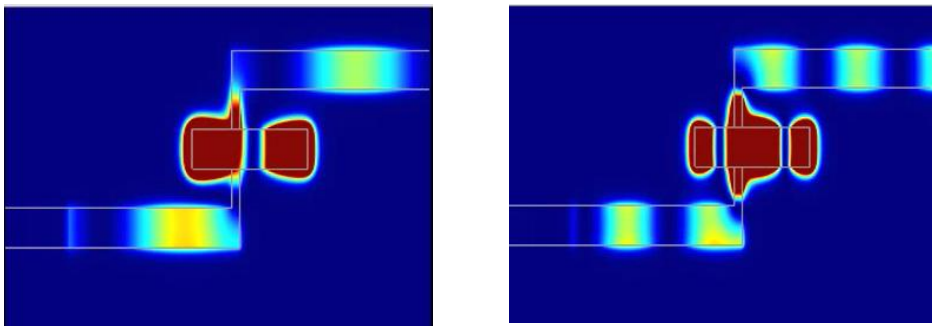

(a) (b)

Fig. 2. The steady-state magnetic field distribution (H_z) of the structure of Fig. 1(a) for (a) the first and (b) the second resonance modes in Fig. 1(b).

The dimensions of the geometrical parameters of the structure of Fig.1(a) are given in Table 1.

Table 1. Preferred dimensions of the structure of Fig. 1(a).

Width of waveguides, W	Width of stubs, g	Length of stubs, k	Width of resonator, W	Length of resonator, L	Distance between the centers of the stubs and resonators, X=ΔL=L/8
100 nm	32 nm	100 nm	100 nm	416 nm	52 nm

For the position of the stubs between $X=\Delta L=0$ and $X=\Delta L=L/4$, the normalized transmission of the structure for different values of $X=\Delta L$ has been compared in Fig. 3 which complies well with the previous explanations.

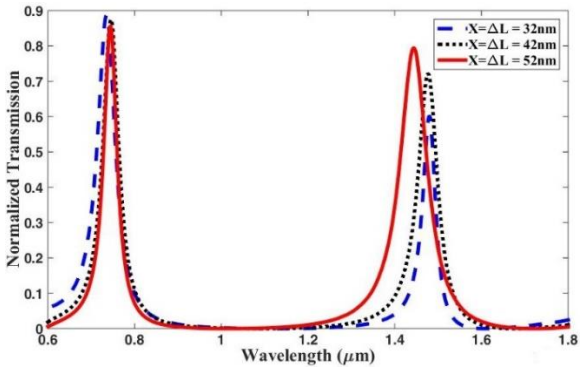

Fig. 3. The normalized transmission spectra of the proposed structure of Fig. 1(a) for different values of the position of the stubs (X=ΔL).

The slot cavity with a width of 100nm is filled with a nonlinear Kerr material, Ag:BaO composite, with linear refractive index of 1.41 [42], the spectrum of the real part of the effective refractive index of which is shown in Fig. 4. For the two wavelength ranges of 1200nm-1800nm

and 600nm-900nm, the real part of the effective refractive index are respectively around 1.72 (1.71-1.73) and 1.74 (1.73-1.75). Therefore, according to Eq. 1, the first and the second resonance wavelengths of the structure are around 1431nm and 724nm, respectively. As shown in Fig. 1(b), the resonance wavelengths which are obtained from the numerical simulation are 1437nm and 732nm, respectively. Therefore, the results derived by analytical method complies well with those of numerical methods.

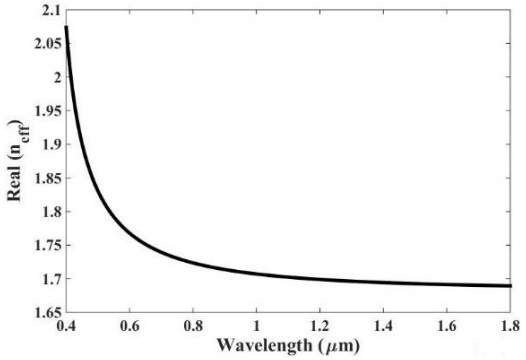

Fig. 4. The spectrum of the real part of the effective refractive index of a plasmonic cavity which has a width of 100nm, filled with a nonlinear Kerr material, Ag:BaO composite, and the linear refractive index of which is 1.41.

3 An ultra-fast all-optical plasmonic dual-band OFF-ON switch based on Kerr nonlinear effect

To achieve the switching operation, the cavity is filled with a nonlinear Kerr material of Ag:BaO composite [42]. In a nonlinear Kerr material, the refractive index increases due to the self-phase modulation (SPM) effect which is caused by a high intensity incident wave. The relation between the signal intensity and the refractive index is: $n = n_0 + n_2 I$, where I is the light intensity, n_0 is the linear refractive index and n_2 is the nonlinear refractive index coefficient that is related to the third-order nonlinear susceptibility χ^3 via: $n_2 = \left(3Z_0\chi^3\right)/\left(4n_0\right)$, where Z_0 is the free space wave impedance [43]. The values of n_0 and χ^3 for this nonlinear material are 1.41 and 6.72×10^{-15} $\mathrm{V^2/m^2}$, respectively [42].

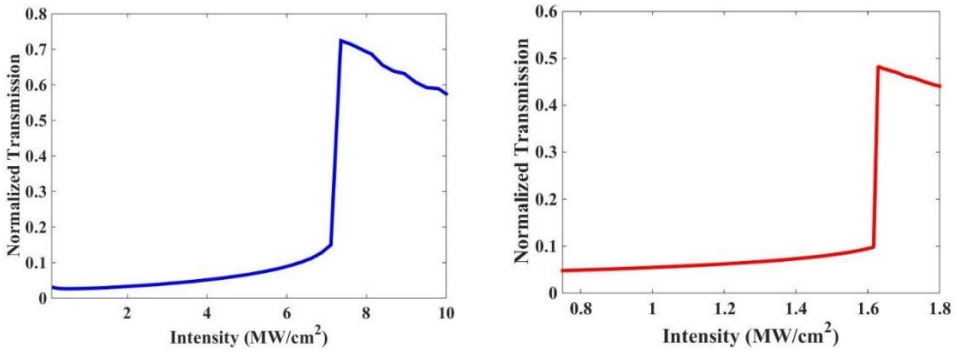

Fig. 5. The normalized transmission versus intensity for the proposed switch of Fig. 1 (a), at wavelengths of (a) λ_1=1550nm and (b) λ_2=850nm .

To obtain a dual-band OFF-ON switching operation, the length of the resonator, given in Table 1 is set in a way that the two resonance peaks occur at wavelengths slightly lower than the two

telecommunication windows of 1550nm and 850nm and the transmissions at these two windows are near zero (OFF-state). This status is obtained when the input wave intensity is low. By applying a high intensity input signal, a red shift in the transmission spectrum occurs. Therefore, increasing the intensity of the incident light, I, results in an increase in the normalized transmission at the two telecommunication windows of 1550nm and 850nm (ON-state). The low and high values of the normalized transmission for the first and the second resonance modes at the OFF-State and ON-State are respectively about 0.025, 0.05 and 0.7, 0.5. The switching mechanism, depicted in Fig. 5, demonstrates the performance of the dual-band all-optical OFF-ON plasmonic switch based on Kerr nonlinear effect. In addition, it is evident that the threshold light intensity required for the switching for the first and the second resonance modes are less than $8.00\,\mathrm{MW/cm^2}$ and $1.70\,\mathrm{MW/cm^2}$, respectively, which is far less than the breakdown values of the used dielectrics [38, 44-46].

To achieve the transmission spectra of Fig. 5, at a specific input intensity, at the first and the second resonance modes, the envelopes of the input signals are assumed to be constant, as shown in Fig. 6(a). The resultant time domain normalized transmission for the input signal intensity of $1.7\,\mathrm{MW/cm^2}$ for the second resonance mode is shown in Fig. 6(b). The steady state value of the normalized transmission obtained from Fig. 6(b) is the same as that of in Fig. 5(b) for the input signal intensity of $1.7\,\mathrm{MW/cm^2}$. From Fig. 6(b), it is apparent that the value of the steady state transmission is about 0.47 and the response time of the switch is about 0.25ps, which shows an ultrafast performance, comparable to other similar switches [38, 44-47]. The switching time is calculated without considering the negligible delay time of the Kerr nonlinear effect of the medium, thus it only originates from the feedback of the structure. In our structures, the optical Kerr material is Ag:BaO composite with an ultrafast nonlinear response time of 0.210 ps [42]. Hence, the results exhibit that the proposed structure can be used in the femtosecond switching applications.

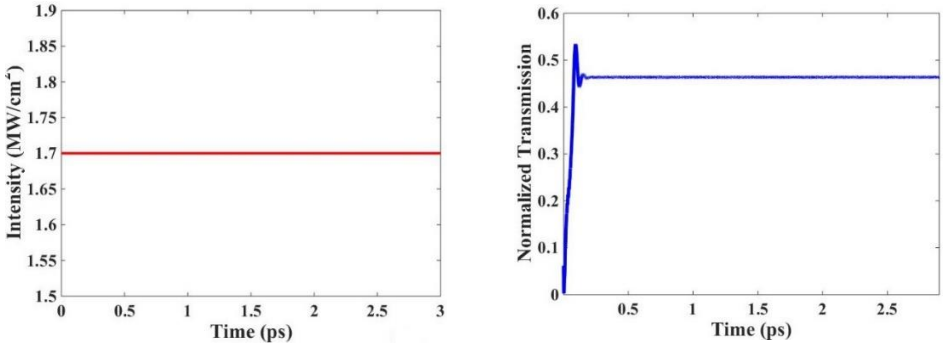

(a) (b)

Fig. 6. Calculation of switching time of the proposed structure: (a) Envelope of the time domain input signal intensity at the second resonance mode (λ_2=850nm) and (b) Envelope of the time domain output signal of the proposed structure.

4 An ultra-fast all-optical plasmonic OFF-ON switch based on the bistability effect

We have also investigated the bistability effect for the proposed switch of Fig. 1(a). Optical bistability is a nonlinear phenomenon which occurs in the presence feedback in a physical structure. In this phenomenon, the transmission of the structure at a certain wavelength has two different stable values for a specific input intensity inside the bistability loop. In other words, the system has two different stable responses at one input intensity [48]. Figure 7 indicates the

bistability loop for the proposed structure of Fig. 1(a) at the second resonance mode (λ_2=850nm).

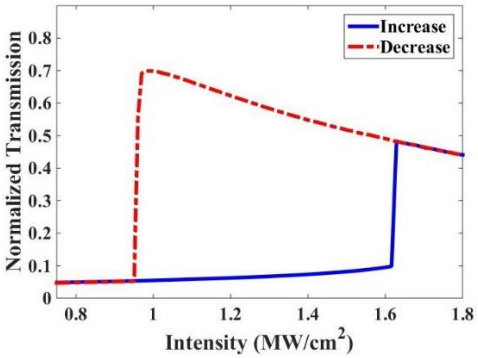

Fig. 7. Bistability loop of the proposed structure of Fig. 1(a) at the second resonance mode (λ_2=850nm).

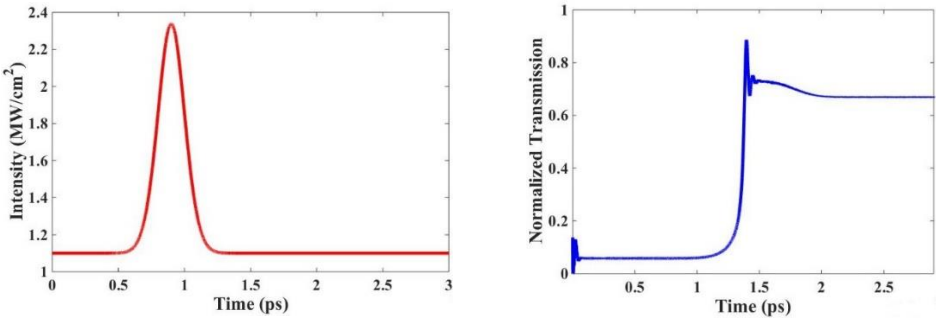

(a) (b)

Fig. 8. Calculation of switching time of the bistability phenomenon in the proposed structure: (a) Envelope of the time domain input signal intensity at the second resonance mode (λ_2=850nm) and (b) Envelope of the time domain output signal of the proposed structure.

According to the result in Fig. 7, the structure has a wide bistability loop at the second resonance mode at telecommunication window of 850nm. Therefore, the switching functionality can also be realized by the optical bistability effect. According to Fig. 7, for an incident wave intensity inside the bistability loop, the normalized transmission can be set to one of the two stable values. For example, for an input signal intensity of $1.1\mathrm{MW/cm^2}$, the normalized transmission can be set to 0.055 (OFF-state) or 0.67 (ON-state). To obtain these two values, which are values inside the bistability loop, the time domain applied input signal envelope is the summation of a constant and a Gaussian signal, as shown in Fig. 8(a). The resultant time domain normalized transmission is shown in Fig. 8(b). The two steady state values of the normalized transmission before and after applying the Gaussian pulse shown in Fig. 8(b), are 0.055 (OFF-state) and 0.67 (ON-state). In other words, by applying the input Gaussian pulse, the switching operation occurs. It is obvious that the transmission of the signal light (850 nm) jumps from 0.055 to 0.67 for the input Gaussian pulse, which shows a significant switching operation. In addition, the switching time response is about 1.5 ps. The extinction ratio is defined as [38]:

$$\mathrm{Ext.R\,(dB)}=10\log\left(\frac{P_{out}^{ON}}{P_{out}^{OFF}}\right) \tag{5}$$

where, P_{out}^{ON} and P_{out}^{OFF} are the output power when the switch is ON or OFF, respectively. Here, we calculate the extinction ratio for the OFF-ON switches inside the bistability loop. From our simulation results in Fig. 7 and Eq. (5), the extinction ratio of our all-optical switch is 10.86 dB which is far higher than those in [38, 44-46].

5 An ultra-fast all-optical plasmonic bi-directional switch

We have also designed an all-optical bi-directional switch by adding another nonlinear cavity to the previous structure, the schematic view of which is shown in Fig. 9(a). The structure operates based on increasing the incident wave intensity which causes the input power to switch between the two output ports. The normalized transmission spectra for this structure are shown in Fig. 9(b). Here, our goal is to design the switch at the first telecommunication window (the second resonance mode: λ_2=850nm). However, from Fig. 9(b), one can see that this structure can also operate as a switch at the first resonance mode of λ_1=1550nm . To display the normalized transmission in Fig. 9(b) around the second resonance mode (λ_2=850nm) more clearly, we have shown the spectra in Fig. 9(c).

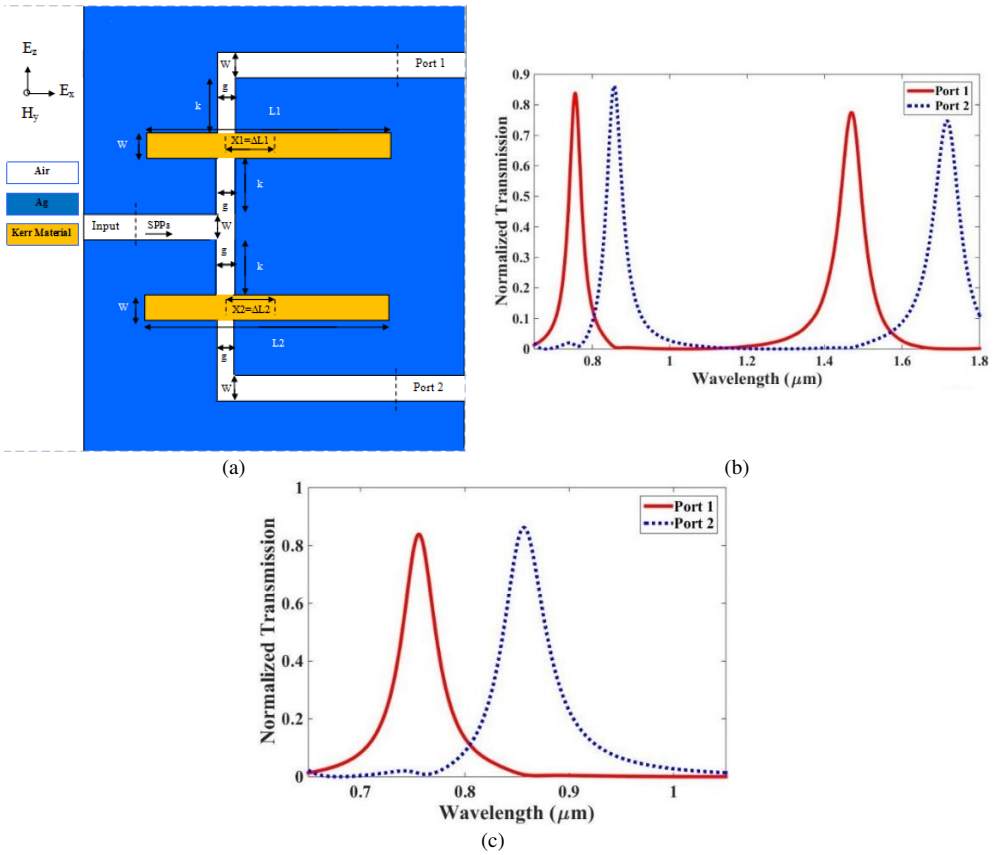

Fig. 9. (a) The two-dimensional building block of the proposed bi-directional switch structure. Normalized transmission spectra of the structure for (b) low input signal intensity and (c) part of (b) around the second resonance mode.

Here, we have set the length of the second cavity so that the peak of the normalized transmission for the second resonance mode occurs at the first telecommunication window of 850 nm. In addition, we have set the length of the first cavity so that the peak of the normalized transmission for the second resonance mode occurs at a wavelength lower that the first

telecommunication window (λ_2=754nm) and the normalized transmission amplitude at λ_2=850nm is near zero (0.002). In other words, when the input signal intensity is low the input power at the wavelength of 850nm only transfers to the second port. The lengths of the cavities of this structure are set as L_1=416nm and L_2=496nm (Fig. 9(a)).

By applying a high intensity input signal, a red shift in transmission spectra occurs. Consequently, increasing the intensity of the incident light, *I*, results in an increase (decrease) in the normalized transmission amplitude to a higher (lower) value at the first (second) output port. In other words, when the input signal intensity is high enough, the input power only transfers to the first port (at λ_2=850nm). The switching mechanism is shown in Fig. 10.

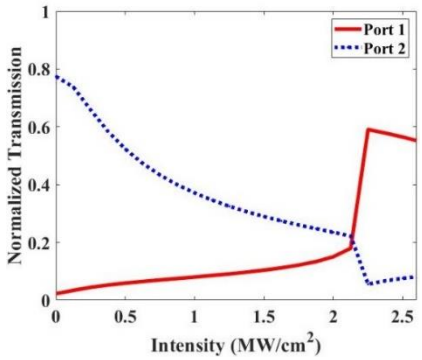

Fig. 10. The normalized transmission versus input intensity for the proposed structure of Fig. 9(a), for the first (solid red line) and the second (dotted blue line) output ports.

Table 2. Comparison of our structure with other references.

Reference		Wavelength (nm)	Intensity ((MW/cm^2))	Response Time (ps)	Dimensions (nm×nm)	Bistability	Bistability Extinction Ratio (dB)
[38]		1115	24.2	0.150	120×930	Yes	3.01
[44]		820 1545	300	0.300	632×529	Yes	3.68
[45]		1310 1550	15	0.500	1870×1010	Yes	8.69
[46]		1482 1538	250	0.300	950×537	Yes	3.68
[47]		1550	2.8	0.380	1400×1700	Yes	11.46
[49]		670, 680 692, 700	560	-	430×560	No	-
This Study	(OFF-ON switch)	850 1550	1.8 8.0	0.250	416×500	Yes	10.86
	(bi-directional switch)	850	2.4	0.360	496×900	No	-

The required light intensity for switching operation is as low as less than $1.8\,MW/cm^2$ and $8.0\,MW/cm^2$ for the first and the second resonance modes for the OFF-ON switch, respectively, and less than $2.5\,MW/cm^2$ for the bi-directional switch. For our proposed OFF-ON switch, the structure has smaller dimensions and for the bi-directional switch, though it has two output ports, dimensions of the structure are comparable to those of [38, 44-47]. In Table 2, our results are compared with those of some other references.

6 Conclusion

In this study, two ultra-fast all-optical plasmonic switches based on metal-insulator-metal (MIM) plasmonic waveguides side-coupled to cavities by stubs have been proposed. The effect of the position of the input and output stubs (the displacement from the center of the rectangular cavity) on the transmission spectra of the structures has been investigated. Consequently, the position of the input and output stubs has been set to design the suitable switches at two telecommunication windows of 1550 nm and 850 nm. To achieve the all-optical switching operation, the cavities are filled with a nonlinear Kerr material of Ag:BaO composite. The refractive index of the nonlinear Kerr material is altered due to the self-phase-modulation (SPM) effect. The switching mechanism based on both nonlinear phenomenon and also the bistability effect, by varying the input signal intensity has been explained and investigated for the proposed structures. The first proposed structure acts as a dual-band plasmonic switch and the second proposed structure works as a bi-directional switch. Both structures are ultra-compact and have significant switching performance and picosecond response time (ultra-fast switching). Our proposed structures have several advantages such as simple fabrication, easy integration, and subwavelength mode confinement. Therefore, the proposed all-optical switches have potential of significant applications in photonic integrated circuits.

Declarations

Competing Interests

The authors have no relevant financial or non-financial interests to disclose.

Conflict of Interest

The authors have no conflicts to disclose.

Author Contributions

The idea of this research article is based on M.R. Pav's M.S. thesis, which was developed with the help of S. Pooretemad. Pav and Pooretemad conducted all the simulations, while all the steps were supervised by Prof. N. Granpayeh and they used his guidance in all stages. The manuscript was written by Pooretemad and Pav, and edited by prof. Granpayeh, who also reviewed the pictures, simulation results, and formulas.

Funding

The authors declare that no funds, grants, or other support were received during the research and preparation of this manuscript.

Availability of data and materials

Data sharing not applicable to this article as no datasets were generated or analyzed during this research.

References

[1] D. K. Gramotnev and S. I. Bozhevolnyi, “Plasmonics beyond the diffraction limit,” Nat. Photonics, vol. 4, pp. 83-91, 2010.

[2] J. Zhang and L. Zhang, “Nanostructures for surface plasmons,” Adv. Opt. Photonics, vol. 4, pp. 157-321, 2012.

[3] G. Veronis and S. Fan, “Modes of subwavelength plasmonic slot waveguides,” J. Light. Technol. vol. 25, pp. 2511-2521, 2007.

[4] B. Zhu, M. Chen, Q. Zhu, G. Zhou, N. M. Abdelazim, W. Zhou, S. V. Kershaw, A. L. Rogach, N. Zhao and H. K. Tsang, "Integrated plasmonic infrared photodetector based on colloidal HgTe quantum dots," Adv. Mater. Technol. vol. 4, p.1900354, 2019.

[5] Y. Fu, X. Hu, C. Lu, S. Yue, H. Yang and Q. Gong, "All-optical logic gates based on nanoscale plasmonic slot waveguides," Nano Lett. vol. 12, pp. 5784-5790, 2012.

[6] A. Tunlz, "Nanoscale nonlinear plasmonic in photonic waveguides and circuits," Riv. Nuovo Cimento, Vol. 44, PP. 193-249, 2021.

[7] M. P. Nielsen, X. Shi, P. Dichtl, S. A. Msier, and R. F. Oulton, "Giant nonlinear response at a plasmonic nanofocus drives efficient four-wave mixing over micron length scales," Science, Vol. 358, PP. 1179-1181, 2018.

[8] A. Campos, N. Troc, E. Cottanich, M. Pellari, H. C. Weissker, J. Lerme, M. Kociak, and M. Hillenkamp, "Plasmonic quantum size effects in silver nanoparticles are dominated by interfaces and local enviroments," Nat. Phys, Vol. 15, PP. 275-280, 2019.

[9] C. Ciraci, R. T. Hill, J. J. Mock, Y. Urzhumov, A. L. Fernandez-Dominguez, S. A. Maier, J. B. Pendry, A. Chikoti, and D. R. Smith, "Probing the ultimate limits of plasmonic enhancement," Science, Vol. 337, PP. 1072-1074, 2012.

[10] W. Shin, W. Cai, P. B. Catrysse, G. Veronis, M. L. Brongersma and S. Fan, "Broadband sharp 90-degree bends and T-splitters in plasmonic coaxial waveguides," Nano Lett. vol. 13, pp.4753-4758, 2013.

[11] S. Pooretemad, M. R. Pav, Z. Ghattan and N. Granpayeh, "Ultra-compact all-optical plasmonic switch for three telecommunication windows using a nonlinear Kerr material and Fano resonance," Appl. Opt. vol. 62, pp. 4123-4133, 2023.

[12] S Khani, M. Danaiean and P. Rezaei, "Modeling of two-dimensional nanoscale Y-bent plasmonic waveguides with cavities for demultiplexing of the telecommunication wavelengths," Plasmonics. vol. 14, pp. 53-62, 2019.

[13] S. Pooretemad, A. Malekijavan and M. Aslinezad, "Ultrawideband bandstop filter based on Fano resonance and rectangular resonators," Appl. Opt. vol. 60, pp. 4266-4272, 2021.

[14] M. R. Pav, N. Granpayeh, S. P. Hosseini and A. Rahimzadegan, "Ultracompact double tunable two-channel plasmonic filter and 4-channel multi/demultiplexer design based on aperture coupled plasmonic slot cavity," Opt. Commun. vol. 437, pp. 285-289, 2019.

[15] X. Lin and X. Huang, "Numerical modeling of a teeth-shaped nanoplasmonic waveguide filter," J. Opt. Soc. Am. B. vol. 26, pp. 1263-1268, 2009.

[16] A. Sumimura, M. Ota, K. Nakayama, M. Ito, Y. lshii and M. Fukuda, "Low-return-loss plasmonic multiplexer with tapered structure," IEEE Photon. Technol. Lett. vol. 28, pp. 2419-2422, 2016.

[17] A. Rahimzadegan, N. Granpayeh and S. P. Hosseini, "Improved Plasmonic Filter, Ultracompact Demultiplexer, and Splitter," J. Opt. Soc. Korea. vol. 18, pp. 261-273, 2014.

[18] J. Li, H. Ye, Z. Yu and Y. Liu, "Design of broadband reciprocal optical diode in a silicon waveguide assisted by silver surface plasmonic splitter," Opt. Express, vol. 25, pp. 19129-19136, 2017.

[19] P. B. Johnson and R. W. Christy, "Compact flexible multifrequency splitter based on plasmonic graded metallic grating arc waveguide," Opt. Lett. vol. 43, pp. 1898-1901, 2018.

[20] S. Asgari, S. Pooretemad and N. Granpayeh, "Plasmonic refractive index sensor based on a double concentric square ring resonator and stubs," Photonics Nanostructures-Fundam. Appl. vol. 42, p. 100857, 2020.

[21] Z. Zhang, L. Luo, C. Yue, W. zhang and S. Yan, "Fano resonance based on metal-insulator-metal waveguide coupled double rectangular cavities for plasmonic nanosensors," Sensors, vol. 16, pp. 642(1-10), 2016.

[22] Z. D. Zhang, R. B. Wang, Z. K. Zhang, J. Tang, W. D. zhang, C. Y. Xue and S. B. Yan, "Electromagnetically induced transparency and refractive index sensing for a plasmonic wavwguide with a stub coupled ring resonator," Plasmonics, vol. 12, pp. 1007-1013, 2017.

[23] X. Zhao, Z. Zhang and S. Yan, "Tunable Fano resonance in asymmetric MIM waveguide structure," Sensors, vol. 17, pp. 11494(1-8), 2017.

[24] M. R. Rakhshani, "Refractive index sensor based on concentric triple racetrack resonators side-coupled to metal–insulator–metal waveguide for glucose sensing," J. Opt. Soc. Am. B. vol. 36, pp. 2834-2842, 2019.

[25] M. Kauranen and A. V. Zayats, "Nonlinear plasmonics," Nat. Photonics, vol. 6, pp. 737-748, 2012.

[26] T. Nurmohammadi, K. Abbasian and R. Yadipour, "Ultra-fast all-optical plasmonic switching in near infra-red spectrum using a Kerr nonlinear ring resonator," Opt. Commun. vol. 410, pp. 142-147, 2018.

[27] A. Tuniz, S. Palomba and C. M. de Sterke, "Pulse length dependent near-infrared ultrafast nonlinearity of gold by self-phase mogulation," Appl. Phys. Lett. vol. 117, p. 071105, 2020.

[28] Y. Shan, Z. Li, B. Ruan, J. Zhu, Y. Xiang and X. Dai, "Two-dimensional Bi_2S_3-based all- optical photonic devices with strong nonlinearity due to spatial self-phase modulation," Nanophotonics, vol. 8, pp. 2225-2234, 2019.

[29] S. Ahadi and N. Granpayeh "Femtosecond all-optical switching based on asymmetric plosmonic Kerr Fabry-perot resonator," Opt. Commun. vol. 349, pp. 36-41, 2015.

[30] S. Kumar and M. Sen "Integrable all-optical switch for photonic integrated circuits," J. Opt. Soc. Am. B. vol. 38, pp. 611-620, 2021.

[31] G. A. Wurtz, R. Pollard and A. V. Zayat, "Optical bistability in nonlinear surface-plasmon polaritonic crystals," Phys. Rev. Lett. vol. 97, p. 057402, 2006.

[32] A. Christos, C. Ciraci and D. R. Smith, "Enhanced optical bistability with film-coupled plasmonic nanocubes," Phys. Rev. Lett. vol. 104, p. 063108, 2014.

[33] K. Zhang and L. Gao, "Optical bistability in graphene-wrapped dielectric nanowires," Opt. Express, vol. 25, pp.13747-13759, 2017.

[34] Q. M. Ngo, K. Q. Le, and V. D. Lam, "Optical bistability based on guided-mode resonances in photonic crystal slabs," J. Opt. Soc. Am. B. Vol 29, pp. 1291-1295, 2012.

[35] S. A. Maier, Plasmonics: Fundamentals and Applications, Springer, 2007.

[36] H. U. Yang, J. D. Archangel, M. L. Sundheimer, E. Tucker, G. D. Boreman and M. B. Raschke, "Optical dielectric function of silver," Phys. Rev. B. vol 91, p. 235137, 2015.

[37] Z. Zhang, J. Yang, X. He, J. Zhang, J. Huang, D. Chen and Y. Han, "Plasmonic Refractive Index Sensor with High Figure of Merit Based on Concentric-Rings Resonator," Sensors, vol. 18, pp. 18010116 (1-14), 2018.

[38] L. Huaiqing, R. Guobin, G. Yixiao, Z. Bofeng, L. Haisu, W. Beliei and J. Shuisheng, "Ultrafast and low-power all-optical switch based on asymmetric electromagnetically tnsparency in MIM waveguide containing Kerr material," Opt. Commun. vol. 353, pp. 189-194, 2015.

[39] F. Hu, H. Yi and Z. Zhou, "Band-pass plasmonic slot filter with band selection and spectrally splitting capabilities," Opt. Express, vol. 19, pp. 4848-4855, 2011.

[40] M. R. Pav, S. P. Hosseini, N. Granpayeh and A. Rahimzadegan, "Application of ultracompact aperture-coupled plasmonic slot cavity with spectrally splitting capability," J. Nanophotonics, vol. 12, p. 016010, 2018.

[41] F. Hu and Z. Zhou, "Wavelength filtering and demultiplexing structure based on aperture-coupled plasmonic slot cavities," J. Opt. Soc. Am. B, vol. 28, pp. 2518-2523, 2011.

[42] Q. F. Zhang, W. M. Liu, Z. Q. Xue, J. L. Wu, S. F. Wang, D. L. Wang and Q. H. Gong. "Ultrafast optical Kerr effect of Ag–BaO composite thin films," Appl. Phys. Lett. vol. 82, pp. 958-960, 2003.

[43] Y. shahamat and M. Vahedi, "Pump-tuned plasmon-induced transparency for sensing and switching applications," Opt. Commun. vol. 401, pp. 40-45, 2017.

[44] T. Nurmohammadi, K. Abbasian and R. Yadipour, "Ultra-fast all-optical plasmonic switch in near infra-red spectrum using a Kerr nonlinear ring resonator," Opt. Commun. vol. 410, pp. 142-147, 2018.

[45] Y. Kong, R. Lin, Q. Wei, C. Liu and S. Wang, "Active dual-wavelength optical switch-based plasmonic demultiplexer using metal-Kerr nonlinear-metal waveguide," IEEE Photonics J, Vol. 9, PP. 1-8, 2017.

[46] T. Nurmohammadi, K. Abbasian and R. Yadipour, “Ultra-fast all-optical plasmon induced transparency in MIM waveguide containing two Kerr nonlinear ring resonator,” J. Opt. vol. 20, p. 055504, 2018.

[47] X. Wang, H. Jiang, J. Chen, P. Wang, Y. Lu and H. Ming, “Optical bistability effect in plasmonic racetrack resonator with high extinction ratio,” Opt. Express, vol. 19, pp. 19415-19421, 2011.

[48] C. Li, Nonlinear Optics Principle and Applications, Springer, 2017.

[49] Z. He, H. Li, S. Zhan, B. Li, Z. Chen and H. Xu, “Tunable multi-switching in plasmonic waveguide with Kerr nonlinear resonator,” Sci. Rep. Vol. 5, pp. 1-9, 2015.